EXPERIMENTAL AND NUMERICAL INVESTIGATION OF COOLANT MIXING IN A MODEL OF REACTOR PRESSURE VESSEL DOWN-COMER AND IN COLD LEG INLETS

by

Ezddin HUTLI*, Valer GOTTLASZ, Istvanne FARKAS, Gyorgy EZSOL, and Gabor BARANYAI

Thermo-Hydraulics Department, Centre for Energy Research,
Hungarian Academy of Sciences, Budapest, Hungary

Original scientific paper
https://doi.org/10.2298/TSCI140915121H

Thermal fatigue and pressurized thermal shock phenomena are the main problems for the reactor pressure vessel and the T-junctions both of them depend on the mixing of the coolant. The mixing process, flow and temperature distribution has been investigated experimentally using particle image velocimetry, laser induced fluorescence, and simulated by CFD tools. The obtained results showed that the ratio of flow rate between the main pipe and the branch pipe has a big influence on the mixing process. The particle image velocimetry/planar laser-induced fluorescence measurements technologies proved to be suitable for the investigation of turbulent mixing in the complicated flow system: both velocity and temperature distribution are important parameters in the determination of thermal fatigue and pressurized thermal shock. Results of the applied these techniques showed that both of them can be used as a good provider for data base and to validate CFD results.

Key words: *mixing, thermal fatigue, pressure vessel, turbulent, coolant, particle image velocimetry, laser induced fluorescence, CFD*

Introduction

The mixing process is important for many accidents that may take place during reactor operation such as reactivity insertion, overcooling transients, thermal stress (TS), and pressurized thermal shock (PTS). Mixing process is of relevance even for normal reactor operation, *e. g.* for determination of the coolant temperature distribution at the core inlet in the case of partially switched off main circulation pumps [1]. When two streams with a strong temperature difference mix (such as in the residual heat removal cycle of a reactor), a strong density gradient also exists. Understanding how density interfaces affect the mixing of coolant streams is integral to predict areas susceptible to thermal fatique (TF) [2]. The fatigue arises from oscillating stresses in the wall that are coupled with the expansion and compression of the material due to oscillating temperatures. When two fluid streams of significantly different temperatures mix before reaching homogeneity, they can expose a section of pipe wall to periodic fluctuations of temperature and potentially facilitate fatigue cracking. Since the oscillating temperature leads also to PTS, the knowledge of transient temperature distribution in the down-comer (DC) is necessary to predict thermal gradients in the structural components of the reactor pressure vessel (RPV) wall [2, 3].

* Corresponding author, e-mail: ezddinhutli@yahoo.com

The two major problems that limit nuclear reactors lifetime are the phenomenon of TF and PTS. The TF being defined as a state (failure) caused by TS. The severity of the failure depends on the shape of the components, the fluid mixing mechanism and the temperature distribution. It is an important phenomenon in nuclear power plants (NPP) management considerations and safety assessment. After many TF events that have recently occurred in various NPP, the focus of thermal striping studies included both fast breeder reactors (FBR) and light water reactors [4-6]. Good examples of TF events in NPP are those of the French FBR in 1992 and PWR in 1998, the Japanese PWR in 1999 and in 2003 [3, 4, 6]. As the RPV, is overcooled by a rapid cooling (*i. e.* thermal shock), there is a drop in the pressure of the primary coolant loop. This rapid decrease in the pressure of the primary coolant causes the high pressure injection pumps in the emergency core cooling (ECC) system to automatically inject coolant into the primary loop. As the injection of coolant repressurizes the RPV, the vessel is subjected to pressure stresses. The stresses exerted on RPV by overcooling and repressurization causes PTS. The PTS phenomenon could be limited by improving the mixing process quality in the system [7]. As it is presented by IAEA, the non-uniform temperature and velocity fields in the reactor DC also can influence overall system behavior (especially circulation rates in individual loops). Because even in case of a uniform temperature field significant flow rate differences might occur in DC therefore the mixing process will be affected, the 2-D modeling of the reactor DC for the system thermal hydraulic analyses is recommended by IAEA [8].

The high cycle turbulence (mixing) effects are not appropriately detectable by common thermocouple instrumentation thus we need to find another suitable tool to detect them. Because of the lack of thermocouples, many researchers investigated TF and PTS phenomenon and the related factors numerically and/or experimentally, based on the fluid mixing phenomena in the T-junction and its effects on the mixing mechanism in complex system in power plant [8-15]. High techniques such as PIV technique associated with the thermocouples network were also used in this field [5, 16-19].

This paper presents the investigation work on the flow field and the temperature distribution near the DC cold-leg inlets and at the ECC (emergency core cooling system). The measurements and calculations have been performed on plexi-glass mock-up in various positions T-junction have been measured, illustrated, and quantified by experimental and numerical approaches on the test model (the half of DC is modelled by a rectangular tank, fig. 1) using particle image velocimetry (PIV), planar laser-induced fluorescence (PLIF), and CFD. The T-junction was selected because it is a common component in the cooling systems of most NPP that has a high exposure of TF. In order to investigate the influence of elbow configuration on the mixing process, the flow behavior in two main pipes were tested but only the results related to the main pipe with elbow configuration are presented here because of the limited space. The comparison has been done between the results obtained by PIV, PLIF, and CFD. The expected outcome of this work is that, guide-lines will be developed from the obtained results to provide a validated basis for future CFD calculations of pipe systems in NPP.

Facility and experimental part

In order to use the symmetry in the used model, the DC is turned into a plane sheet as in the photo in fig. 1. One half of DC is modelled by a rectangular tank. Three pipes connected to the tank are modelling the cold-legs. There is a smaller pipe joining to one of these pipes. This smaller pipe is modelling the ECC inlet mimicking the VVER-440 reactor's geometry. The whole model is built of plexi-glass so it is optically measurable. The photo and geometry of test section are presented in figs. 1 and 2, respectively. Table 1 presents the geometrical properties of the model and the real NPP. Table 2 presents the flow conditions for the model and also for the real NPP. In this work,

a 2-DPIV and PLIF techniques were used to measure the flow field and temperature distribution. The experimental conditions are presented in tab. 2. The temperature difference between two pipes was fixed at 20 °C (40 °C in the main pipe and 20 °C in the branch pipe). The tested parameters are given in tab. 3. The PIV measurements have been done in many cross-sections as shown in fig. 2, the reason for focusing on the area of the T-junction at the ECC (on the cold leg, on the T-junction at the cold leg and the DC) is that the mixing processes at these positions have a large effect on TF. The temperature differences at T-junction have been measured, illustrated, and quantified by experimental and numerical approach on Tee-test model in various positions, fig. 2, and configurations using PLIF and CFD. The CFD calculations were performed using the Fluent code to simulate the turbulent fluid behavior, in particular, to determine the velocity field and temperature distribution in the fluid at the same interrogation areas as that in the experimental work. The generation of the geometry model was done based the best practice guidelines (BPG). In order to obtain high accuracy of solutions using the suggestions of BPG for the use of CFD in a nuclear reactor safety applications we developed a structured mesh of hexahedral elements consisting 4 milion nods, with special care for meshing around ECC line/cold leg and cold legs/DC connections. Based

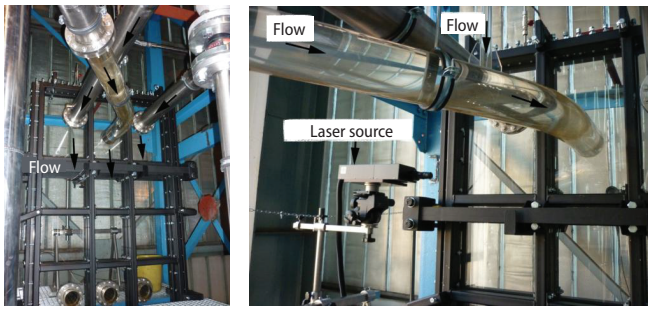

Figure 1. Photos of the test rig; half of the DC is modelled by a rectangular tank, three pipes connected to the tank are modelling the coldlegs

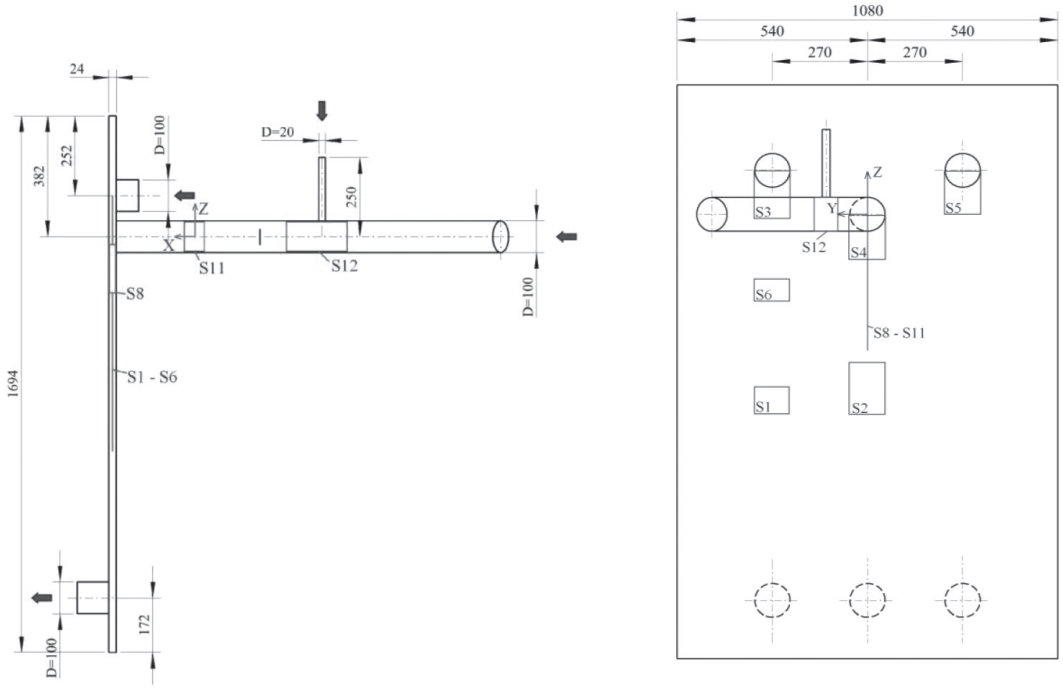

Figure 2. The PIV and PLIF measurement cross-sections [mm]

Table 1. Geometry of parts of the Paks NPP and the model

Geometry part	Paks NPP	Model
Diameter of the cold leg	492 mm	100 mm
Size of the half DC (width × depth)	5376 × 121 mm	1080 × 24 mm
Height of the DC	7710 mm	1554 mm
DC height above the inlet	987 mm	249 mm
Inner diameter of the ECC pipe	111 mm	22 mm
ECC nozzle position from the inner wall of the DC	3350 mm	670 mm
Length of the cold legs	-	2000 mm

Table 2. Experimental conditions for PIV, LIF measurements and CFD calculations

Condition name	Cold leg		ECCs pipe		Flow rate ratio (FRR%) $(q/Q)\times100$	Cold leg temperature [°C]	ECC temperature [°C]
	Q [m^3h^{-1}]	V [ms^{-1}]	q [m^3h^{-1}]	V [ms^{-1}]			
A	6.3	0.2228	2.6	2.3	42%	40	25
B	6.3	0.2228	1.6	1.415	25.4%	40	20
C	3.2	0.1132	1.6	1.415	50%	40	20
D	3.2	0.1132	0.8	0.7	25%	40	20

Table 3: Testing parameters in PIV, LIF measurements, and CFD calculations

Parameter name	Paks NPP	Model
Q (cold leg flow rate)	300 kg/s	0,5-3 kg/s (per loops)
q (ECC flow rate)	28 kg/s	0,01-1 kg/s
Cold leg temperature	267 °C	40 °C
ECC temperature	55 °C	20 °C

on the Reynolds numbers and the preliminary calculations we applied k-ω SST turbulence model with second order discretization scheme which is able to describe high Reynolds number flows. Near the walls we used the Enhanced wall function. The pressure at the bottom of the DC model was the outlet boundary condition and uniform velocity profiles were assumed as inlets of the four pipes (three cold legs and one branch pipe). These profiles were calculated from the measured flow rates. Close attention was paid to the completeness of the geometry: all important local geometrical features were included in the model. However, not all recommendations of the BPG could be considered for grid quality because of geometry complexity. The grid angle below 20° and over 160° was avoided. The non-dimensional wall distance y^+ was calculated and tested in order to be in the limit which is presented by BPG. The PIV and LIF procedures are presented in previous work [20]. For the different cross-sections different measurement arrangements are necessary. Figure 3 shows the set-up of the tools (camera

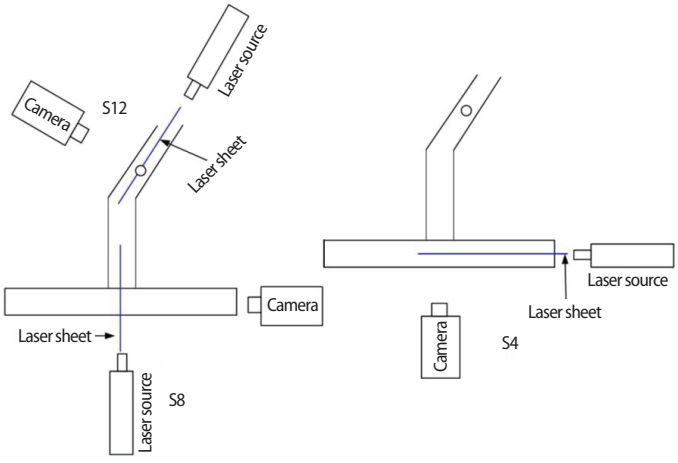

Figure 3. The PIV and LIF visualization system arrangements

and the laser) to perform the measurements at S4, S8, and S12 cross-sections, respectively. In order to avoid the reputation only the results of these three cross-sections are presented. The results are qualitatively interpreted and visualized and no overall uncertainty analysis was made. However, the error range of the velocity magnitudes can be well approximated by measuring the flow rate at a well-known cross-section of the loop. In this way the averages of the measured velocities could be compared. The relative uncertainty maximum proved to be about 5%. This can be assigned to the limitations of measuring the 2-D projection of the particle velocities in the flow field. In case of LIF measurements the accuracy basically depends on the quality of calibration process. The calibration was made and the accuracy of the thermometers at the inlet and the outlet of the test rig were used as a reference which is ±0.15 °C of full scale. The maximum resolution of the temperature obtained by LIF is 0.23 °C as the intensity of a pixel can change between 1 to 255 (8 bit). Repetition has been done for calibration process and measurements in order to minimize the influence of test rig vibration on the results. More information about the PIV errors and LIF calibration is presented in previous work [20].

Results and discussion

Velocity distribution – PIV measurements and CFD calculations

The flow visualization test in the T-junction using PIV technique was carried out with parameters related to flow rate ratio (FRR) between two pipes (branch and main pipe, q and Q, respectively, as in tab. 2). As it was mentioned earlier, it is difficult to fully understand the mixing mechanism of the fluid through the mere visualization of the entire flow field, therefore a small region around the T-junction was selected to measure close-up flow-field data (PIV, PLIF, and CFD have been made on the same region). This visualization displays origins of the average velocity in the T-junction area. Figures 4(a)-4(c) shows the average flow pattern (average velocity vector map) in the T-junction which is characterized by the jet behavior exiting from the branch pipe. The used working conditions are A, C, and D, tab. 2. The jet was bent in the direction of the main flow of the main pipe (effect of high upstream flow velocity of the main pipe). Increasing the flow rate of the main pipe, the bend of the jet increases *i. e.* jet penetration decreases. The jet penetration depends also on the flow rate of the branch pipe itself [5, 17]. But in general the expected forms of the jet depend on the *FRR* between both pipes ($FRR = (q/Q)\times 100\%$).

This could be classified into four patterns: (1) wall jet (low *FRR*, not presented here), (2) re-attached jet, (3) deflecting jet (*FRR* as given in tab. 2), and (4) impinging jet obtained by the increasing flow in the branch pipe, thus depending on the momentum/velocity ratio of the entering flows from branch and main pipe, the turbulent mixing patterns can be classified and defined clearly. The existing elbow after the T-junction (branch pipe) and before the DC entrance (T-junction at the DC) enhances the mixing process [5, 16, 19]. Three parameters are used to investigate the structure of the jet and mechanisms: average velocity distribution in x- and in z-direction plus average velocity. The average velocity distribution contains information about the average structure of the jet, while the average velocity displays the area with the highest variation in the jet structure which is not presented here but it could be deduced and understood from velocity vector maps in figs. 4(a)-4(c). For each condition around 1000 frames were used to evaluate the mixing flow mechanism and the average velocity. This is the reason why one can not see any kind of vortices on the velocity vector map (the average is presented). The influence of the flow rate of the branch pipe on the mixing process can be understood from the comparison between the results obtained with condition (C) and that with condition (D). Figures 4(b) and 4(c) show that the jet thickness and penetration increase as the jet flow rate increases. The bending of the jet by main flow coming from the main pipe decreases with the

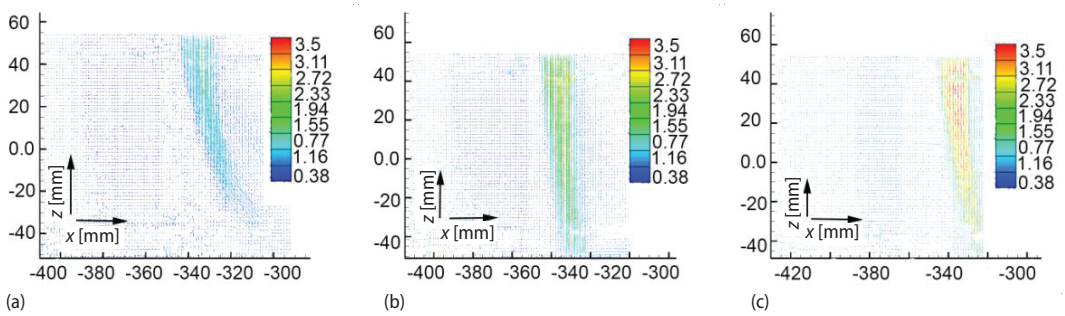

Figure 4. The PIV velocity distributions [ms^{-1}] obtained under working conditions A, C, and D, respectively (*for color image see journal web site*)

increase of the jet flow rate. Figures 5-8 show the comparison between the velocity profiles in x- and z-direction extracted from PIV and CFD results at certain cross-sections. The comparison shows good qualitative agreements while quantitatively it is not good for velocity in z-direction (V_Z), figs. 5 and 6. In figs. 7 and 8 we can see that the maximum velocity is recorded at the center because the profile is in the center of ECC pipe where the maximum velocity position should be (flow from ECC pipe). The velocity distribution along the chosen profile in interrogation area under T-junction between two pipes (ECC and cold leg) and that under the junction between the main pipe (cold leg) and the pressure vessel is qualitatively well predicted in the CFD calculations. Figures 9(a)-9(c) shows the average velocity vector map obtained by PIV measurements at cross-section S4 in the T-junction at DC entrance under three different working conditions (A, B, and C, respectively). From figs. 9(a) and 9(b) we can deduce the influence of branch pipe flow rate on the velocity distribution at DC inlet. A maximum velocity appears at azimuthal position in the inlet of RPV. The analysis of the two vector maps, figs. 9(a) and 9(b), reveals that the ratio between the two flow rates has significant influence on the velocity distribution *i. e.* on the mixing process. The highest velocity is recorded on the left side as it appears in both figs. 8(a) and 8(b), this asymmetrical distribution is a result of the elbow configuration in the main pipe, fig. 2. The asymmetricity is a consequence of the interaction between the flow from the main pipe and that from the branch pipe in addition when water, passes through a pipe elbow, the bend will cause the fluid particles to change their main direction of motion. There will be an adverse pressure gradient generated from the curvature with an

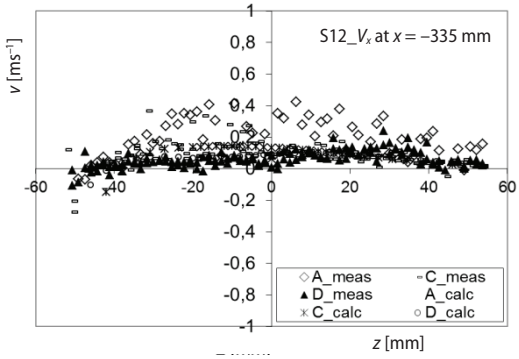

Figure 5. Profiles of the velocity components in x-direction (PIV and CFD)

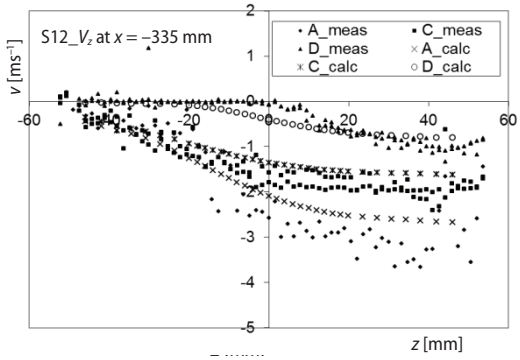

Figure 6. Profiles of the velocity components in z-direction (PIV and CFD)

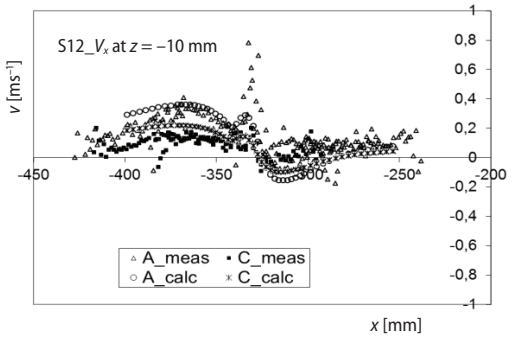

Figure 7. Profiles of the velocity components in x-direction (PIV and CFD)

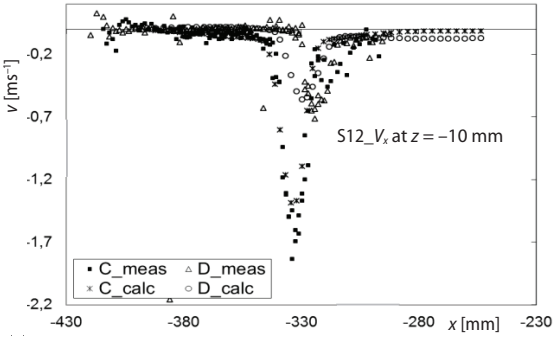

Figure 8. Profiles of the velocity components in z-direction (PIV and CFD)

increase in pressure, therefore a decrease in velocity close to the convex wall, and the contrary will occur towards the outer side of the pipe. The interaction between centrifugal and viscous forces creates a strong secondary flow in the plane normal to the pipe axis. This secondary flow consists of two counter-rotating vortices, one in either half of the pipe cross-section. They flows of opposite sign the resultant path lines followed by the fluid particles are helical, fig. 10, [21, 22]. Generally, in figs. 9(a)-9(c) the average velocity is higher in the T-connection in the lower arc of the main pipe (fluid shedding area) and in the border under the arc. This also related to the elbow configuration in plus the gravity force (accelerates the flow).

The bend in the cold leg pipe far from the RPV inlet nozzle causes an asymmetric velocity profile at the RPV inlet, it means that a part of the fluid remains almost unmixed. Therefore the temperature distribution will have inhomogeneous character at that area.

The flow in the cold leg with that from the ECC injection nozzle create the flow stratification in the cold leg which influences mixing process in DC. Since the density of liquid is constant, the momentum is playing the essential role in the mixing process in all sections. The momentum ratio between the main and branch pipe can be varied by the two parameters, velocity ratio and branch pipe diameter according to eq. (1) [23].

$$M_R = \frac{\rho_m V_m (D_m - D_b)}{\rho_b V_b \pi \left(\frac{D_b}{2}\right)^2} \tag{1}$$

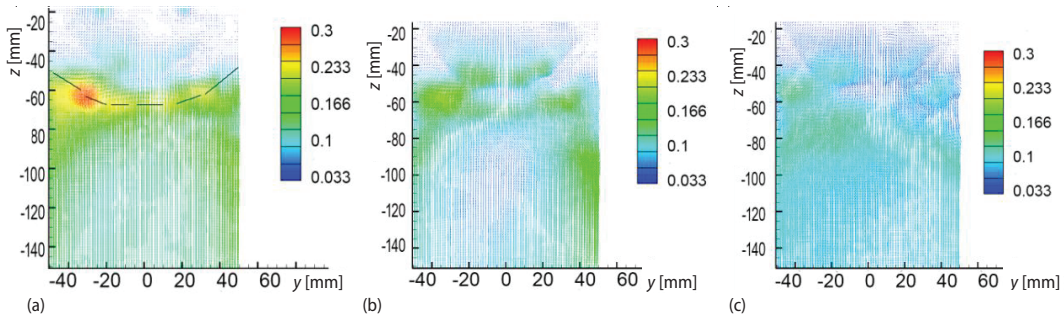

Figure 9. The PIV velocity distributions [ms^{-1}] obtained at S4 position under working conditions A, B, and C, respectively, the dashed line in (a) is the pipe border (pipe cross-section is above the line) (*for color image see journal web site*)

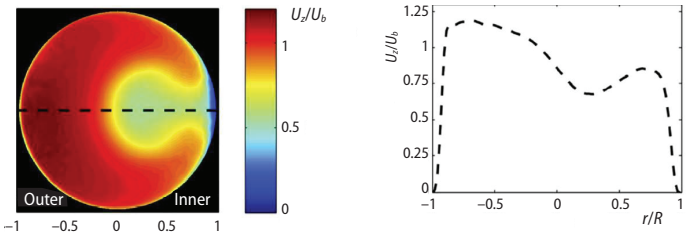

Figure 10. Example of the stream-wise velocity (U_z) distribution at the exit of a 90° pipe bend;
(a) contour map of the stream-wise velocity field at a pipe cross-section, (b) profile of the stream-wise velocity scaled by the bulk speed (U_b) along the horizontal axis [22]
(*for color image see journal web site*)

where M_R is the momentum ratio, ρ_m and ρ_b – the fluid densities for the main flow and branch flow, respectively, V_m and V_b – the mean velocity of the main and branch flow, respectively, D_m and D_b – the main and branch pipe diameters, respectively.

These two parameters (velocity ratio and branch pipe diameter) provide different mechanisms for the mixing phenomena and we used the flow rate instead of these two parameters. The effects of *FRR* (*i. e.* velocity ratio) are evaluated to study the mixing mechanism. Figures 11 and 12 show the velocity ratio effects on the average velocity distribution in the interrogation area. The increasing of the branch velocity leads to an increasing of the average velocity at RPV, fig. 9. This result proofs that the effect of branch pipe diameter on the momentum ratio is the most important parameter for improving the operating conditions of the mixing mechanism [5]. The comparison between figs. 9(b) and 9(c) shows the influence of the main pipe flow rate. The *FRR* for condition B, fig. 9(b), was $FRR = (q/Q)\times 100\% = 25.4\%$ while for condition C, fig. 9(c), it was $FRR = 50\%$. In general, the coolant flow in the junction area between the cold leg and the DC appeared to be non-uniform with a low velocity region below the cold-leg inlet nozzle. The downward velocity profile developed into a non-uniform shape as it flows downstream in DC, this non-uniform temperature and velocity fields in the reactor DC can influence overall system behavior (especially circulation rates in individual loops) [8]. The comparison reveals that the increase in *FRR* is enhancing the mixing process, figs. 9(b) and 9(c). The velocity distributions are more homogeneous in fig. 9(c) than in fig. 9(a) and 9(b). The minimum and maximum velocity recorded in case C is 0.033 and 0.1, respectively, while for case A the velocity was 0.033 and 0.33 m/s and for case B the velocity was 0.033 and 0.16 m/s. From these results, one can say that there is an optimum *FRR* which can lead to get high mixing

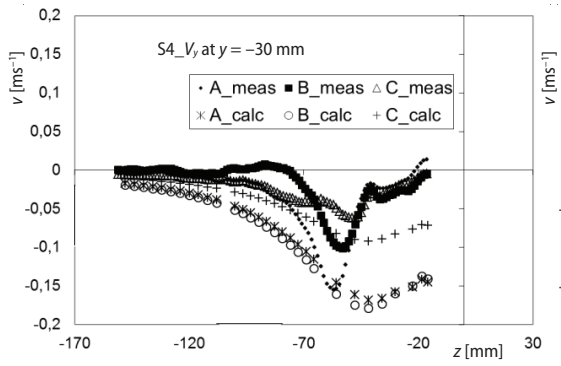

Figure 11. Profiles of the velocity components in y-direction on the left side of the inlet of DC at the main pipe (PIV and CFD)

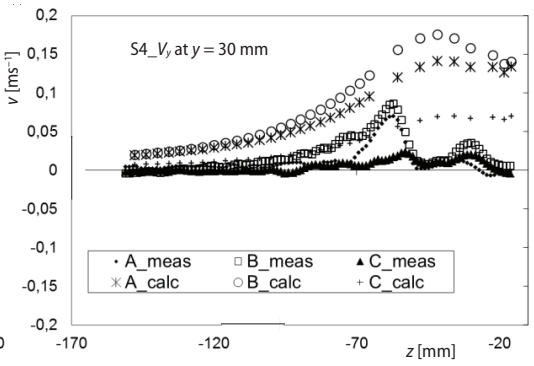

Figure 12. Profiles of the velocity components in z-direction on the left side of the inlet of DC at the main pipe (PIV and CFD)

rate leading to optimum (desirable) velocity distribution in the system. In other words, the design of such cooling system should take into consideration of the mixing process. Figures 11 and 12, show the velocity profiles of V_y and V_z obtained by PIV measurement results and calculated using CFD. The agreements are clear between these results. The existence of deviation in some points can be acceptable because the flow is complex and normally there is an error which could originate from both techniques (PIV and CFD). This deviation needs further investigation. As mentioned in the publications, the discrepancies could be due to the integrated effects of many complex flow phenomena such as wake-wake, wake-vane, and vane-boundary layer interactions occurring simultaneously in complex flow environment as we have here [24, 25]. In addition, the deviations between PIV and CFD results appearing in the figures are results of the wall friction (the pipe roughness is an important factor to this phenomenon) and of the distortion phenomenon: when the illuminated particles are observed through a medium that is optically inhomogeneous due to flow compressibility, the resulting particle image pattern is subjected to deformation and blur. The wall curvature has also influence (cold leg). Also the PIV results could be affected when there are two parallel walls as in case of DC (the model which is used here is a narrow sandwich with 24 mm thickness). Another reason of appearing the deviations is the difficulty to define or determine exactly where is the position of interrogation area in PIV measurements which is needed for CFD calculations. It has big effects on the results especially in the turbulent flow area (example S8), another technical problem is that the characteristic of the laser sheet used is not completely uniform (it has serpentine lines). Assessing the accuracy of the PIV measured data using empirical and theoretical correlations, needs further study. The repetition of both the calibration process and the measurements (average should be used) were necessary in this work to get results with high accuracy. Figures 13(a)-13(c) show the results obtained by PIV measurements at S8 under the conditions A, B, and C, respectively. The influence of the flow rate of both pipes and FRR on the velocity distribution could be understood by comparing the velocity vector maps in figs. 13(a)-13(c). The average map of the velocity distribution of the three cases presented in fig. 13 could be a consequence of that in fig. 9. The difference between the maximum velocity recorded at S8, fig. 13, and that which is recorded at S4, fig. 9, could be related to the gravity force which speeds up the fluid at section S4. Quantitative comparison between the PIV and CFD results shows a good agreement, see figs. 14, and 15.

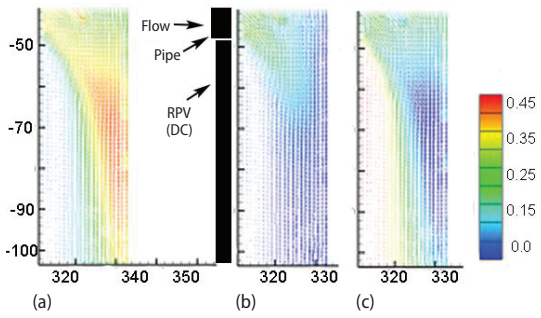

Figure 13. The PIV velocity distributions [ms^{-1}] obtained at S8 position under working conditions from left to right (a), (b), and (c), respectively (*for color image see journal web site*)

Temperature distribution, LIF measurements and CFD calculations

The temperature differences at Tees have been measured using PLIF, illustrated and quantified by experimental approaches on Tee-test models in various positions and configurations, CFD calculations were made under the same conditions. The results presented here are the averages of a few hundred measurements (frames) for each working condition and CFD output. Thus the expected errors are practically eliminated. The measurements and calculations have been made based on conditions given in tab. 2. Figures 16 and 17 show the PLIF and

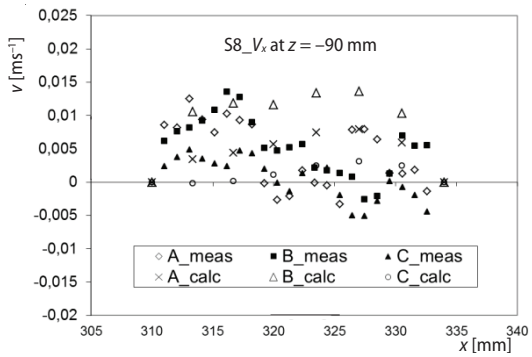

Figure 14. Profiles of the velocity components in x-direction (PIV and CFD)

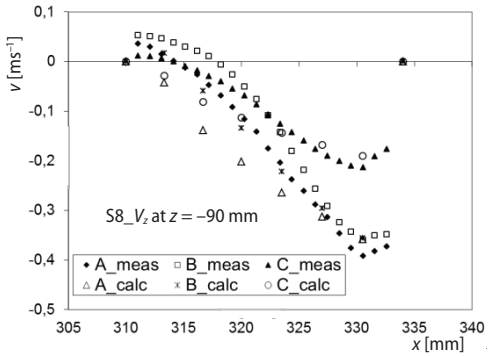

Figure 15. Profiles of the velocity components in z-direction (PIV and CFD)

CFD results, respectively, obtained under working conditions A, B, and C, tab. 2, (note that the CFD results are mirrored). The results of both PLIF and CFD techniques show that the highest temperature appears around the jet. In the bottom we can see the average (mixed) temperature value recorded as a result of the jet penetration. The mixing area in the images is the area which has average temperature values according to the scale associated with each image in figs. 16 and 17. As a result of the temperature difference between the branch pipe and the main pipe, the average structure of the jet could be easily noticed. By decreasing the flow rate of the branch pipe (condition B in tab. 2), the flow from the main pipe bents the jet which leads to decreased jet penetration. The comparison between PLIF and CFD results shows a good agreement (qualitatively and quantitatively), the maximum and minimum temperature values are identical and in general the temperature distribution obtained by both techniques is almost identical, both techniques (PLIF and CFD) present the back flow phenomenon in the bottom of the images in figs. 16 and 17 but in the CFD results it is clearer. Comparison between figs. 16(a), 16(b), 17(a), and 17(b) gives highlights on the influence of the flow rate of the branch pipe on temperature distribution and the mixing flow process.

Figure 16(c) shows the results obtained with working condition C, tab. 2. In this figure the jet appears with less bend because the flow from the main pipe is decreased. Figures 16(b), 16(c), 17(b), and 17(c) give highlights on the influence of the flow of the main pipe on the temperature distribution and mixing phenomenon in the tested area. The analysis of the results in figs. 16(a)-16(c) and figs. 17(a)-17(c) reveals that the momentum ratio between the main and branch pipes velocities

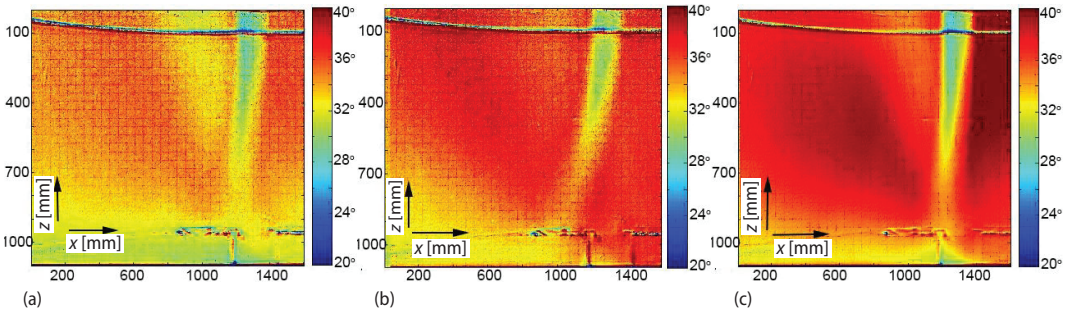

Figure 16. The PLIF temperature distribution [°C] obtained at S8 position under working conditions A, B, and C, respectively
(*for color image see journal web site*)

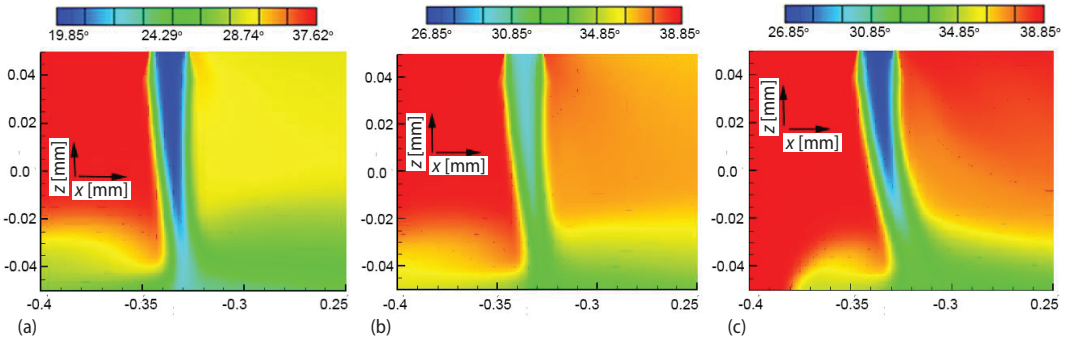

Figure 17. The CFD temperature distribution [ms^{-1}] obtained at S8 position under working conditions A, B, and C, respectively
(*for color image see journal web site*)

is the most useful parameter for classifying the fluid mixing mechanism, which includes both the velocity and pipe diameter characteristics of the main and branch pipes. In addition, the effects of flow rate (velocity when diameter is kept constant) on the fluid mixing mechanism have shown and explained the behavior of turbulent jets. Considering the geometry, the elbow configuration has effect on the interaction between the jet and the main flow. The significant effect of elbow appears clearly in the velocity and temperature distribution and profiles measured after the elbow [5, 16, 19].

Conclusions

A water experiment using a VVER-440 DC which is modelled by a rectangular tank and a simple T-pipe junction with downstream elbow in the main pipe was carried out to investigate thermal striping phenomena. The PIV, LIF, and CFD techniques were used. The results showed that the flow pattern in DC cold leg T-junction was characterized by the branch pipe jet which acts as a turbulent jet in the connecting main pipe. Various types of jets could appear, depending on the FRR when the pipe's geometries were kept constant. The FRR between the main and the branch pipe were selected to study the mixing flow process before the entrance of the DC in order to minimize the TF risk. Increasing the FRR from 25.4% to 50% enhances dramatically the mixing process. In general, the findings are that, the FRR is an important parameter influencing the mixing phenomenon. The elbow configuration in the main pipe has significant influence on the mixing phenomenon (on velocity and temperature distribution). The comparison between PLIF and CFD results shows a good agreement (qualitatively and quantitatively), the maximum and minimum temperature values are identical. A significant difference can be observed between CFD and PIV results while between CFD and LIF results are more identical. A further CFD work is needed to obtain good results. The PIV and LIF could be good providers for CFD validation. Since these measurements and calculations are carried out under isothermal conditions therefore the obtained results can not draw general conclusion for a real power plants but it can led to understand the mixing process mechanism. The variation of densities between main, branch pipe and DC the gravitational effects could also play a role (gravity force effect) on the mixing process which is not investigated in this work.

References

[1] Rohde, U., *et al.,* Fluid Mixing and Flow Distribution in a Primary Circuit of a Nuclear Pressurized Water Reactor-Validation of CFD Codes, *Nuclear Engineering and Design*, *237* (2007), 15-17, pp. 1639-1655
[2] Eggertson, E. C., *et al*., Turbulent Mixing and its Effects on Thermal Fatigue in Nuclear Reactors, World Academy of Science, *Engineering and Technology*, *76* (2011), 52, pp. 206-2013

[3] Apanasevich, P., *et al.,* Comparison of CFD Simulation on Two-Phase Pressurized Thermal Shock Scenario, *Nuclear Engineering and Design*, *266* (2014), Jan., pp. 112-128
[4] Metzner, K. J., *et al.,* Thermal Fatigue Evaluation of Piping System Tee-Connections (THERFAT), 2007, http://cordis.europa.eu/documents/documentlibrary/97848051EN6.pdf
[5] Hosseini, S. M., *et al*., Classification of Turbulent Jets in a T-Junction Area with a 90-Deg Bend Upstream, *International Journal of Heat and Mass Transfer*, *51* (2007), 9-10, pp. 2444-2454
[6] ***, IAEA-TECDOC-1627, Pressurized Thermal Shock in Nuclear Power Plants: Good Practices for Assessment, Deterministic Evaluation for the Integrity of Reactor Pressure Vessel, International Atomic Energy Agency –Vienna, 2010
[7] Stahlkopf, K. E., Pressure Vessel Integrity under Pressurized Thermal Shock Conditions, *Nuclear Engineering and Design*, *80* (1984), 2, pp. 171-180
[8] ***, IAEA, Guidelines on Pressurized Thermal Shock Analysis for WWER Nuclear Power Plants, IAEA Document IAEA-EBP-WWER-8 (2001).
[9] Faidy, C., Thermal Fatigue in Mixing Areas: Status and Justification of French Assessment Method, *Proseedings*, 3rd International Conference on Fatigue of reactor Components, EPRI-US NRC-OECD NEA, Seville, Spain, 2004
[10] Muramatsu, T., Numerical Analysis of Nonstationary Thermal Response Characteristics for a Fluid-Structure Interaction System, *Journal of Pressure Vessel Technology*, *121* (1999), 3, pp. 276-282
[11] Igrashi, M., *et al.,* Study on Fluid Mixing Phenomena for Evaluation of Thermal Striping in a Mixing Tee, *IAEA-INIS*, *36* (2003), 30, 36067327
[12] Igrashi, M., Study on Fluid Mixing Phenomena for Evaluation of Thermal Striping in a Mixing Tee, 10th International Topical Meeting on Nuclear Reactor Thermal Hydraulic, NURETH-10, Seoul, Korea, 2003
[13] Tanaka, M., Experimental Investigation of Flow Field Structure in Mixing Tee, *Proceedings*, 6th International Conference on Nuclear Thermal Hydraulic, Operation and Safety, ID: N6P334, NUTHOS-6, Nara, Japan , 2004
[14] Hosseini, S. M., Experimental Investigation of Thermal-Hydraulic Characteristics at a Mixing Tee, *Proceedings*, International Heat Transfer Conference, FCV-17, Sydney, Australia, 2006
[15] Kimura, N., *et al.*, Study on Convective Mixing for Thermal Striping Phenomena – Experimental Analyses on Mixing Process in Parallel Triple-Jet and Comparisons between Numerical Methods, *IAEA-INIS*, *33* (2001), 16, 33015236
[16] Ogawa, H., *et al.,* Experimental Study on Fluid Mixing Phenomena in T-Pipe Junction with Upstream Elbow, *Proceedings*, 11th International Topical Meeting on Nuclear Reactor Thermal-Hydraulics (NURETH-11) Popes Palace Conference Center, Avignon, France, 2005
[17] Hosseini, S. M., Visualization of Fluid Mixing Phenomenon, *Proceedings*, 6th International Congress on Advances in Nuclear Power Plants, ICAPP05, ID: 5006 (R006), Seoul, 2005
[18] Aminia, N., Hassan, Y. A., Measurements of Jet Flows Impinging Into a Channel Containing a Rod Bundle Using Dynamic PIV, *International Journal of Heat and Mass Transfer*, *52* (2009), 23-24, pp. 5479-5495
[19] ***,FluentInc.FlowLab1.2,(2007),TurbulentFlowandHeatTransferinaMixingElbow,(2007),pp.1-8.https://www.yumpu.com/en/document/view/3338571/turbulent-flow-and-heat-transfer-in- a-mixing-elbow/6
[20] Hutli, E., *et al.,* Experimental Approach to Investigate the Dynamics of Mixing Coolant Flow in Complex Geometry Using PIV and PLIF Techniques, *Thermal Science, 19* (2015), 3, pp. 989-1004
[21] Homicz, G. F., Computational Fluid Dynamic Simulations of Pipe Elbow Flow, Sandia National Laboratories, Albuquerque, N. Mex., USA, 2004
[22] Kalpakli, A., Experimental Study of Turbulent Flows through Pipe Bends, Technical Reports, Royal Institute of Technology KTH Mechanics, SE-100 44 Stockholm, 2012
[23] Nematollahi, M., *et al.,* Effect of Bend Curvature Ratio on Flow Pattern at a Mixing Tee after a 90 Degree Bend, *International Journal of Engineering*, *3* (1985), Nov., pp. 478-487
[24] Gango, P., Numerical Boron Mixing Studies for Loviisa Nuclear Power Plant, *Nuclear Engineering and Design*, *177* (1997), 1-3, pp. 239-254
[25] Elvis, E. D. O., *et al.,* Experimental Benchmark Data for PWR Rod Bundle with Spacer-Grids, *Proceedings*, CFD for Nuclear Reactor Safety Applications (CFD4NRS-3) Workshop, Bethesda North Marriott Hotel & Conference Centre, Bethesda, Md., USA, 2010

Paper submitted: September 15, 2014
Paper revised: April 7, 2015
Paper accepted: April 25, 2015